

Contactless Biometric Identification using 3D Finger Knuckle Patterns

Kevin H. M. Cheng, Ajay Kumar

Abstract— Study on finger knuckle patterns has attracted increasing attention for the automated biometric identification. However, finger knuckle pattern is essentially a 3D biometric identifier and the usage or availability of only 2D finger knuckle databases in the literature is the key limitation to avail full potential from this biometric identifier. This paper therefore introduces (first) contactless 3D finger knuckle database in public domain, which is acquired from 130 different subjects in two-session imaging using photometric stereo approach. This paper investigates on the 3D information from the finger knuckle patterns and introduces a new feature descriptor to extract discriminative 3D features for more accurate 3D finger knuckle matching. An individuality model for the proposed feature descriptor is also presented. Comparative experimental results using the state-of-the-art feature extraction methods on this challenging 3D finger knuckle database validate the effectiveness of our approach. Although our feature descriptor is designed for 3D finger knuckle patterns, it is also attractive for other hand-based biometric identifiers with similar patterns such as the palmprint and fingerprint. This observation is validated from the outperforming results, using the state-of-the-art pixel-wise 3D palmprint and 3D fingerprint feature descriptors, on other publicly available datasets.

Index Terms— Biometrics, finger knuckle identification, 3d finger dorsal matching, contactless hand identification

1. INTRODUCTION

BIOMETRIC technologies offer enormous potential to meet a range of security requirements for the automated and efficient recognition of humans. Among various biometric identifiers, fingerprint [2], [32] is probably the most widely deployed biometrics for the e-governance, e-business and a range of law-enforcement applications. Other biometric identifiers such as face, iris, palmprint, or vascular patterns have also established their usefulness for a range of applications [1]. The usefulness of biometric identifiers depends on the nature of application requirements including the accuracy, efficiency, and importantly the user convenience.

Several challenges have emerged with the biometric recognition deployments using fingerprints. The degradation in fingerprint matching accuracy due to frequent skin deformations, residual dirt, sweat, moisture and/or scars, is well-known while a large number of manual labourers and elderly population also suffers from fingerprints with less than acceptable quality for the identification. The NIST report in [3] submitted for the US Congress stated that about 2% of the population does not have usable fingerprints. Similar conclusions have also been reported in a large-scale proof of concept study from UIDAI [4] which stated that about 1.9% of subjects cannot be reliably authenticated by using their fingerprints. The finger knuckle patterns can be simultaneously imaged during the fingerprint identification and are less susceptible to damages during daily life activities. The finger knuckle patterns can be more conveniently imaged from a distance, unlike fingerprints, as the major creases and curved patterns are easily visible with naked eyes. In summary, there are reasonable arguments to indicate that the addition of finger

Table 1. Summary of key differences between 2D and 3D finger knuckle identification.

	2D Finger Knuckle Images	3D Finger Knuckle Images
Information and Invariability	Intensity, affected by illumination	Surface Normal / Depth / Curvature, invariant to illumination
Recognition Performance	Medium	High
Identification of Spoof and Alterations	Low	High
Convenience	High	High
Earlier Work	Several promising studies	Almost Nil

knuckle patterns for biometric recognition could address some of the limitations with the usage of only fingerprints.

Finger knuckle patterns are believed to be quite unique in establishing human identities. Several researchers [5]-[8], [10] have investigated discriminative information from finger knuckle patterns using 2D images, and some evidence emerges from the study in [11] which investigated discriminative information from 3D images using conventional *shape index* measurements [12]-[13]. Similar to the palmprints [9, 10], it can be inferred that the most discriminative information from finger knuckle patterns is associated with the knuckle curves and creases. However, accurate extraction of finger knuckle curves and creases using 2D images is quite difficult because the changes in illuminations (*e.g.* caused by uneven reflections from 3D knuckle surfaces in the vicinity) strongly influences the intensity information. It is generally known that the biometric systems incorporating 2D imaging are more prone to spoof attacks (*e.g.* print attacks). A person impersonating another person by presenting a printed image poses serious challenges to preserve the integrity of a biometric system.

• Kevin H. M. Cheng and Ajay Kumar are with the Department of Computing, The Hong Kong Polytechnic University, Hong Kong.

The usage of 3D finger knuckle information (surface normal vector, depth, or curvature) can enable more reliable characterization of finger knuckle patterns as the 3D information is expected to be invariant to the change of illuminations. In addition, the 3D imaging setups generally acquire 2D images and therefore simultaneous usage of 3D and 2D finger knuckle images can be used to achieve a performance that may not be possible when either of such information is employed alone. Printed photograph cannot reveal 3D information and therefore 3D finger knuckle imaging systems can easily detect such spoof attacks. It is extremely difficult to present replicas of 3D finger knuckle patterns as they require subjects to intentionally present their fingers under sophisticated imaging setups, unlike those required for 2D finger knuckle images that can also be acquired covertly. Table 1 summarizes key differences between the potential from 2D and 3D finger knuckle images for automated biometric identification.

Despite many advantages with the usage of 3D finger knuckle features, there are many challenges in the development of an automated 3D finger knuckle biometric system. Firstly, it is difficult to design a feature descriptor, to robustly recover unique information from 3D curve and creases, which can offer more accurate and efficient recognition. Secondly, a key limitation with the emerging 3D scanning technologies to replace conventional 2D systems is associated with their high cost and bulk which can be mainly attributed to the nature of technologies employed for the 3D imaging. For example, five cameras were used in [1] while [14] uses a high-speed camera and a specialized projector to achieve 3D finger scanning. Therefore, there is a strong motivation to develop low-cost imaging solutions for the 3D finger knuckle imaging. Finally, most important bottleneck in the advancement of much needed research efforts on 3D finger knuckle identification is the lack of *any* database in the public domain.

This paper investigates the development of first automated biometric system using 3D finger knuckle patterns. There are several potential areas of applications for such technologies in business, forensics, providing secured access in buildings and installations. This paper also presents a new feature descriptor for matching 3D finger knuckle patterns and attempts to estimate the uniqueness of the 3D finger knuckle patterns. A 3D finger knuckle database is also developed to advance further research efforts in this area.

1.1 Related Work

Study on finger knuckle patterns has attracted attention from many researchers, with many exciting results in the literature for the accurate biometric identification. However earlier attempts have only demonstrated the effectiveness of 2D knuckle patterns/images for the online personal identification and such attempt using 3D knuckle patterns is yet to emerge in the best of our knowledge. Many research efforts to study 3D shape patterns using 3D ear [15], 3D fingerprints [16], and 3D face [17] have resulted in the

development of more accurate or reliable biometric systems. Therefore a comprehensive study on the recovery of 3D knuckle patterns and comparisons of 3D finger knuckle features is highly desirable and has been the focus of our work.

The gray-level 2D knuckle images typically acquire anatomy of skin crease patterns between the middle and proximal phalanges of fingers. A range of approaches using such knuckle images have been detailed in the literature for biometrics based personal identification. Based on the nature of feature descriptors, these approaches can be largely categorized into three categories; those based on subspace learning (e.g. [6], [11]), spectral features (e.g. [18]-[19], [41]) and those based on the discretization of local features (e.g. [8], [20]). Among these, those approaches based on the discretization of local features have attracted more attention in the literature as such methods generate compact size templates, which leads to faster retrieval or matching. Reference [24] provides comparative experimental results, on a range of minor and major knuckle patterns, using publicly accessible database from over 700 different subjects. These results using local feature descriptors achieve outperforming results and is reasonable to incorporate such approach as a baseline to ascertain performance from 2D knuckle images.

1.2 Our Work and Key Contributions

This paper addresses the key limitations of currently available finger knuckle identification technologies by developing a 3D finger knuckle feature extraction and matching model that can simultaneously recover extended finger knuckle features from 3D finger knuckle images reconstructed from a single 2D imaging sensor. Simultaneous availability of 3D information from the finger knuckle images not only offers significantly improved matching accuracy but can also ensure automated detection of sensor-level spoof attacks using printed knuckle images. Any direct application of known or popular 3D feature descriptors, e.g. those designed for other biometric identifiers such as palm or fingerprint, is expected to offer limited performance. Instead, specialized feature extractors should be designed to recover the most discriminative information from the 3D finger knuckle patterns which is largely embedded in 3D curves and creases with varying thickness. Some of the successful attempts in recovering 3D fingerprints using photometric stereo [16] requires reconstruction or the integration of source 3D information, i.e. surface normals. The reconstruction process is generally complex, e.g. popular method used in [21] requires FFT and IFFT which are known for their demanding complexity, and is known to introduce errors in the reconstructed depth images. These errors are introduced as it is difficult to find closed form solutions for the integration, i.e., integrability problem [21]-[22], and mainly results from the discontinuities around irregular ridge valley boundaries during the 3D reconstruction. Therefore, any direct usage of source 3D information from the surface normal vectors

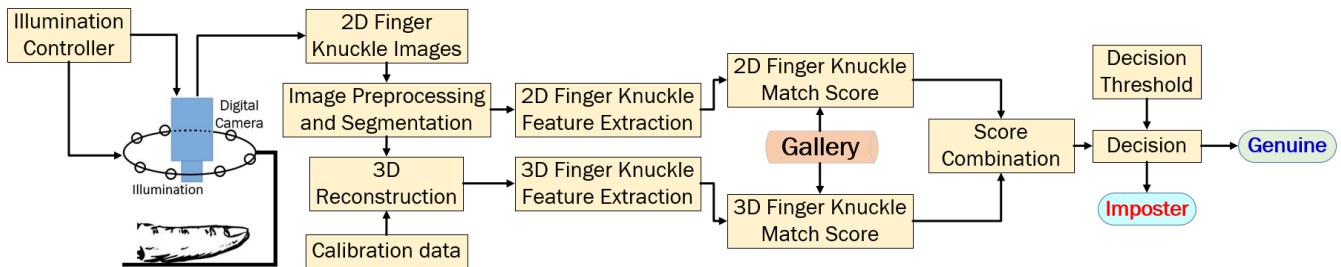


Fig. 1. Block diagram of 3D finger knuckle recognition system.

can not only enhance matching accuracy for 3D knuckle images but can also help to reduce the complexity and is therefore highly desirable. The introduction of new 3D finger knuckle modality also raises a fundamental question on the (theoretical) upper limit on the performance from this biometric modality. Therefore, uniqueness of 3D knuckle patterns needs to be established to answer some of such fundamental questions relating to 3D finger knuckle patterns. The key contributions from this paper can be summarized as follows:

1. This paper investigates and develops a new biometric system using contactless 3D finger knuckle images. Simultaneous acquisition of 3D and 2D finger knuckle images can be used to significantly improve the matching accuracy that may not be possible by using either 2D or 3D finger knuckle patterns alone, and such an approach is presented in this paper. Experimental results presented in this paper indicate that, unlike 2D finger knuckle identification, new 3D finger knuckle identification system can also help to preserve integrity of the biometric system by detecting sensor level print attacks. The individuality of finger knuckle patterns is yet to be studied and therefore we also attempt to answer the fundamental question on the uniqueness of 3D finger knuckle biometric modality. An individuality model presented in section 4 estimates the theoretical upper limit on the expected performance from finger knuckle patterns and would facilitate further research in this area.
2. We develop a new feature descriptor to efficiently and more accurately match 3D finger knuckle biometric patterns. This feature descriptor can efficiently recover and encode the curvature and orientation details and considers their partial-similarity during the matching. Our detailed and comparative experimental results presented in section 5 of this paper indicate outperforming results and validate our approach developed in this paper. Although our feature descriptor is designed for recovering discriminative information from 3D finger knuckle images, it is also useful for other biometric identifiers such as palm and fingerprint. Our comparative experimental results detailed in section 5 in this paper indicate outperforming results, over the

state-of-the-art baselines on public databases, and validate the effectiveness of our feature descriptor.

3. Lack of any publicly available 3D finger knuckle database is one of the key limitations for much needed further research in this area. Therefore, this paper develops the first two-session 3D finger knuckle database. This 3D finger knuckle images database has been acquired from 130 different subjects, with 2820 images, and is made publicly available [40] for researchers to advance much needed further research in this area.

The rest of this paper is organized as follows. Section 2 presents an overview of the 3D finger knuckle identification system using a simplified block diagram. The details for our methodologies, including the proposed feature descriptor, appear in section 3. The uniqueness of finger knuckle patterns is discussed in section 4 with details on the proposed individuality model. The comparative experimental results are systematically presented in section 5 of this paper while the key conclusions from this work are summarized in section 6.

2. SYSTEM OVERVIEW AND BLOCK DIAGRAM

A simplified block diagram for 3D finger knuckle identification system developed in this work is shown in Figure 1. Multiple 2D finger knuckle images are firstly acquired under different illuminations and the acquisition is automatically synchronized using with respective illumination using a computer. The acquired images are then preprocessed and automatically segmented to extract region of interest images. These segmented images, acquired under different illuminations, are then used for estimating surface normal vectors. Unlike other photometric stereo based biometric imaging system (e.g. fingerprint [16], [27]), the complex process of integrating surface normal vectors for recovering the depth images is not required in our system. The 3D finger knuckle features are then directly extracted from the surface normal vectors of 3D finger knuckle images. The 2D finger knuckle image, although noisy as each

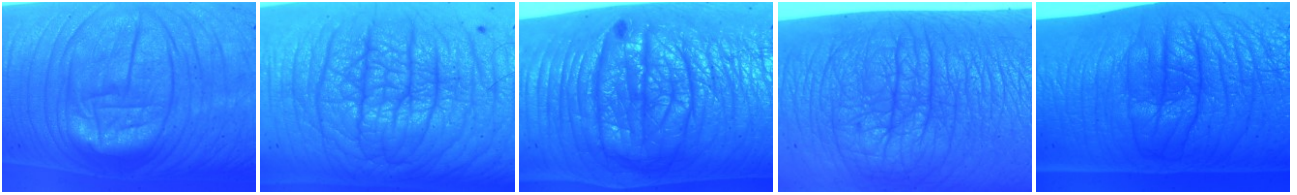


Fig. 2. Sample raw images acquired from different subjects.

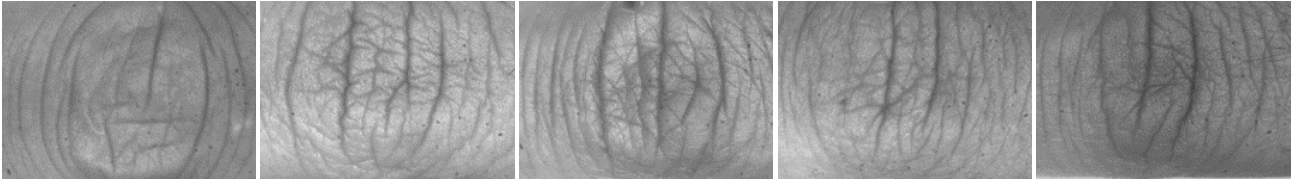


Fig. 3. Sample segmented images acquired from different subjects.

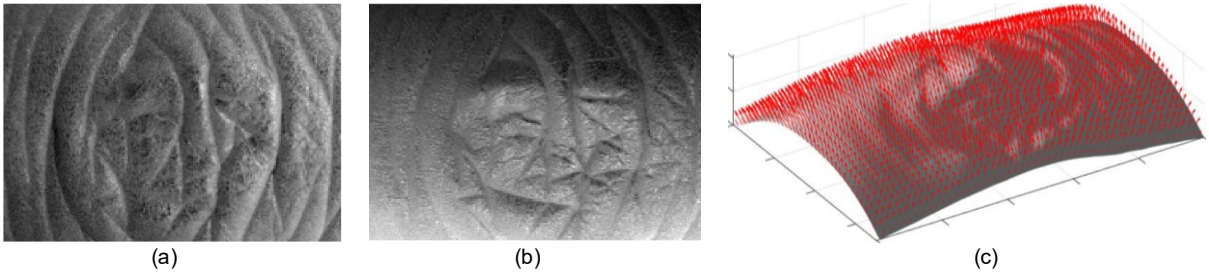


Fig. 4. Sample images of surface gradient: (a) with respect to horizontal direction; (b) with respect to vertical direction; (c) Surface normal vectors.

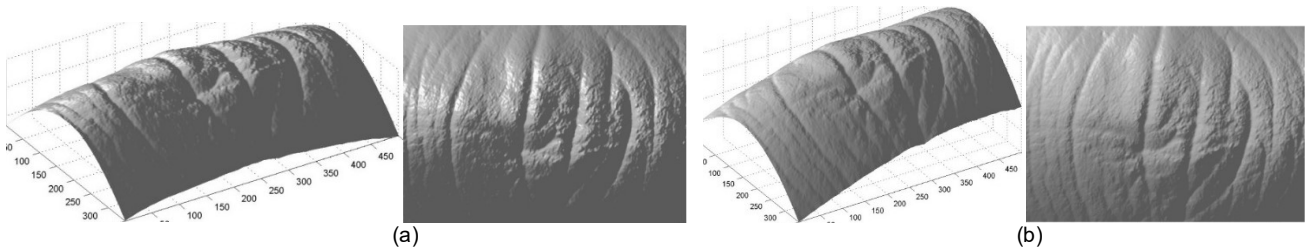


Fig. 5. 3D reconstructed images using: (a) Frankot-Chellappa; (b) Poisson Solver.

of them is acquired under partial illumination, used to recover 3D finger knuckle images can also be utilized to improve match accuracy for the system and is also investigated in our work. The match scores between the probe and gallery pairs are then respectively computed for 3D and 2D finger knuckle images. The final decision to assign an unknown user to either genuine or imposter class is made using the combine match score and its comparison with the decision threshold.

3. 3D FINGER KNUCKLE IDENTIFICATION

In the following subsections, key components of the 3D finger knuckle identification system including the image acquisition, image preprocessing and segmentation, 3D reconstruction, feature extraction steps and the matching process is detailed.

3.1 Image Acquisition

We use photometric stereo approach and imaging setup in

[16] to acquire 3D finger knuckle images. This approach requires a low-cost fixed camera, with seven evenly distributed illuminations surrounding the camera lens, a control or driver circuit to power up the illuminations and any general-purpose computer. The control circuit is programmed to adjust the illuminations while the computer coordinates to synchronize the control circuit during the camera imaging. The positions of the illuminations are approximated by measuring the height and observing the orientation of shadow when a pin is placed at the center of the field of view. Relative positions of the illuminations at every pixel is computed during the calibration of the imaging setup [32]. The finger dorsal region is presented to the camera during the 3D imaging. A number of 3D finger knuckle images are acquired in quick succession while respective light sources are activated. Figure 2 presents sample images acquired from different subjects during the imaging.

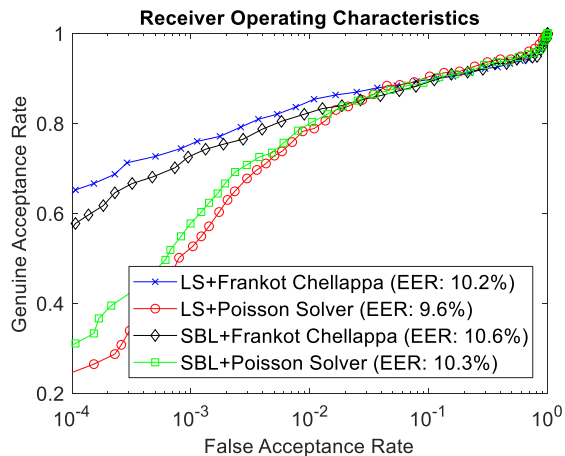


Fig. 6. Comparisons between different reconstruction methods.

3.2 Image Preprocessing and Segmentation

Each of the acquired images are firstly subjected to the segmentation to automatically extract the region of interest images. This is achieved by firstly computing an average image for each set of stereo images, followed by the edge detection. In order to localize the image region containing knuckle patterns, a fixed size of rectangular window is used to probe the edge-detected image in horizontal and the vertical directions. Similar to as in [6], the number of edge pixels within this window is computed. A fixed region of interest is segmented from the image with the maximum number of edge pixels within this sliding window. These segmented images are further subjected to contrast stretching operation and then used for the 3D reconstruction input as detailed in the next section. Figure 3 shows samples from the segmented images of different subjects.

3.3 3D Reconstruction

The 3D surface normal vectors from of the photometric stereo images are recovered using the conventional photometric stereo method [23]. A simplified specular reflection removal approach is adopted to accurately recover the surface normal vectors. For a set of stereo images, 90% of the maximum or highest intensity values are defined as the threshold for the detection of outliers. Intensity values larger than this threshold are considered as the specular values and are automatically discarded. However, when there are too many specular reflection values at a pixel position, at least four lowest intensity values are retained to estimate the surface normal vectors. The finger surface is assumed be Lambertian and we use such assumptions for the traditional photometric stereo approach, as justified in many references *e.g.* [16], [27], to recover 3D surface normal. Let us define $\mathbf{i} = [i_1, i_2, \dots, i_D]^T$ be the intensity values of a pixel corresponding to the D different light sources; $\mathbf{l} = [l_x, l_y, l_z]^T$ be the vector of a light source; $\mathbf{L} = [\mathbf{l}_1, \mathbf{l}_2, \dots, \mathbf{l}_D]^T$ be the matrix of the light sources; $\mathbf{n} = [n_x, n_y, n_z]^T$ be the surface normal vector and ρ be the *albedo*.

$$\mathbf{i} = \mathbf{L} \cdot \mathbf{n} \cdot \rho \quad (1)$$

Surface normal vectors are computed using the least square approximation:

$$\mathbf{m} = \mathbf{n} \cdot \rho = (\mathbf{L}^T \mathbf{L})^{-1} \mathbf{L}^T \mathbf{i} \quad (2)$$

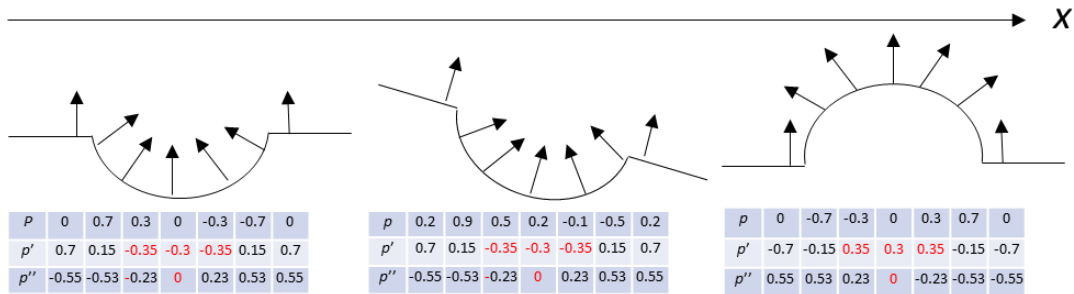
$$\rho = |\mathbf{m}| \quad (3)$$

$$\mathbf{n} = \frac{\mathbf{m}}{|\mathbf{m}|} \quad (4)$$

Figure 4 illustrates sample images corresponding to the surface gradients and surface normal vectors. Traditional 3D feature descriptors [30], [31] extract features *from* the depth images, which can be computed by integrating the surface normal vectors in obtained from equation (4). The *Poisson Solver* [22] and *Frankot Chellappa* [21] approach are two popular approach to recover the depth map while addressing integrability problem. The Poisson Solver approach generated better visual result (Figure 5) that closely resembled with the natural knuckle patterns. However, the usage of *Frankot Chellappa* approach constantly offered consistently better performance. Figure 6 presents such comparative performance evaluation from 105 subjects six forefinger knuckle images, using a two-session protocol that generated 630 genuine match scores and 65520 imposter match scores, with *Surface Code* [30] as the feature descriptor. Please refer to Section 5.1 for more details on the database and experimental protocol. Many state-of-the-art photometric stereo methods, *e.g.* [25]-[26], [28] for the real objects may not be suitable for accurately recovering 3D finger knuckle patterns for the biometric recognition. Our comparative experimental results for the verification performance using SBL [26] and the traditional least square (LS) approach appear in Figure 6. These results can justify the choice of traditional least square approach with *Frankot Chellappa* algorithm for our problem.

3.4 3D Feature Descriptor using Surface Gradient Derivatives

The 3D images generally provide more stable or invariant details and can enable more accurate extraction of finger knuckle curves and creases (as discussed in section 1). Therefore a more specialized feature descriptor to recover and match such 3D information is developed. Among many 3D surface details (*e.g.* surface normal vector, depth, and curvature), 3D feature descriptors for other hand based biometric identifiers, *e.g.* 3D palm, have shown outperforming results using the curvature [30] and depth [31]. These are however not expected to be accurate enough to

Fig. 7. Illustration of the derivatives of gradient p .

extract most discriminative features from the finger knuckle patterns as these are presented in 3D curves and creases with varying profile/thickness. Another more important aspect of the feature descriptor introduced in this work is that the photometric stereo based 3D biometric imaging systems (e.g. fingerprint [16], [27]) computes the depth images by integrating surface normal vectors. In fact, every 'reconstruction algorithm' the surface normal needs to be integrated and suffers from *integrability* problem [9] which can be more severe for 3D knuckle patterns due to the irregular ridge and valley structure. This process is not only known to introduce errors but is also computationally complex. The process of computing curvature information from depth images even requires significant amount of time (shown in section 5.1.1). We therefore attempt to address such limitations by developing a new feature descriptor, which can directly extract discriminative features from the 3D surface normal vectors, alleviating the

need for computing depth or curvature images. The surface normal vectors essentially present source 3D information which is discriminative and also robust to the common photometric variations. Therefore appropriate surface normal vector based measurements can provide significant capabilities for discriminating identities. The feature descriptor introduced in this section is highly discriminative as it can efficiently capture both the line and orientation information using two bits per pixel, which cannot be achieved neither from descriptor in [30] (four-bits per pixel) or in [31] (no orientation information is encoded). We now detail the formulation of this feature descriptor using the source 3D information.

Let r represent the imaged 3D finger knuckle surface. This 3D surface can be explicitly described in terms of a function along 2D coordinates x and y as follows:

$$r = g(x, y) \quad (5)$$

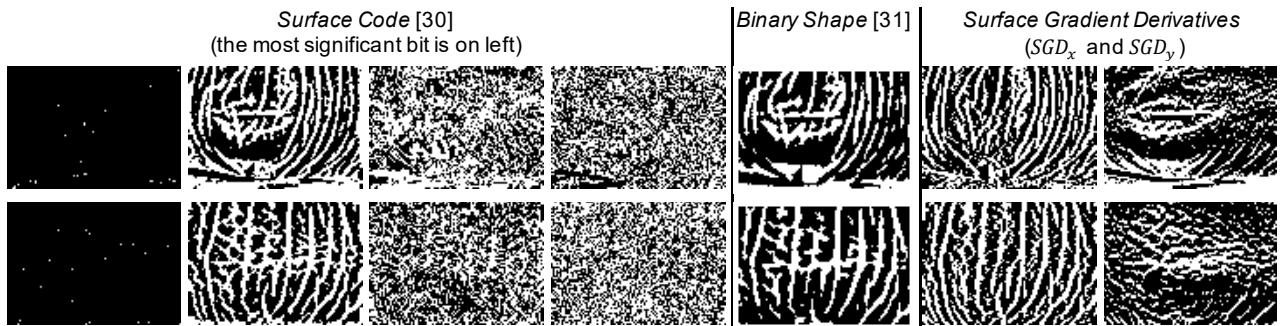
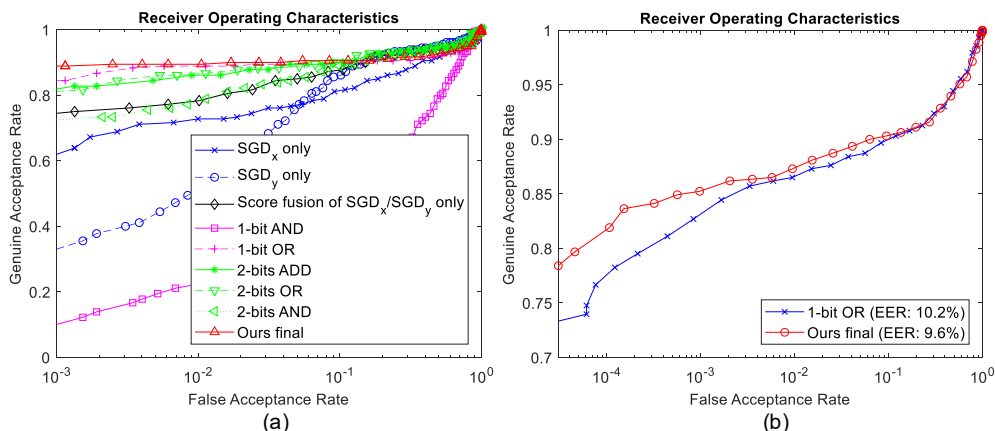
Fig. 8. Sample binary feature images of *Surface Code* [30], *Binary Shape* [31] and proposed *Surface Gradient Derivatives*. Images in a row are from the same subject.

Fig. 9. Comparisons of using various matching schemes (a) 30 subjects; (b) 105 subjects.

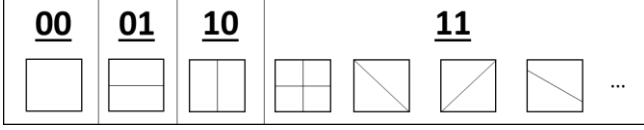


Fig. 10. Schematic representation of the gradient derivative features.

Table 2. Pixelwise surface gradient derivative features mapping function.

$a_{ij} \backslash b_{ij}$	00	01	10	11
00	0.5	1	1	1
01	1	0	1	0.5
10	1	1	0	0.5
11	1	0.5	0.5	0

The surface normal vector \mathbf{n} on this surface r can be expressed as follows:

$$\mathbf{n} = [p, q, 1]^T \text{ where } p = \frac{\partial g(x,y)}{\partial x}, q = \frac{\partial g(x,y)}{\partial y} \quad (6)$$

where p and q represents the gradient of $g(x, y)$ along respective axes. The gradient space is a two-dimensional space containing all points (p, q) [23].

If the surface normal vectors are recovered using photometric stereo approach detailed in section 3.3, unit surface normal vectors in the form of $\hat{\mathbf{n}} = [n_x, n_y, n_z]^T$ are obtained from equation (4). The surface gradients p, q can then be directly computed (without the need of object surface z) as:

$$p = \frac{n_x}{n_z}, q = \frac{n_y}{n_z} \quad (7)$$

Figure 7 illustrates a schematic representation of surface normal vectors (arrows) in a cross-sectional view. In this figure, x-axis is pointing towards the right and we define sample gradients p for the illustration. The derivatives of gradient p with respect to the direction x can be computed as the difference between the neighboring values using a simple gradient function. It can be observed that the valley region is associated with negative values, of the first derivative of gradient p with respect to the direction x , while ridge region is associated with positive values of the first derivatives of gradient p with respect to the direction x . Valley and ridge regions can therefore be easily distinguished by setting zero as the decision boundary. The most discriminative patterns on finger knuckle surface can be identified from the high frequency valley and ridge patterns. Therefore, it is expected that the first derivative of surface gradients can describe discriminative features in finger knuckle patterns.

We can further consolidate the knuckle feature formulation and recover the derivatives of surface gradient variables p, q represented as in the following:

$$\frac{\partial p}{\partial x} = \frac{\partial^2 g(x,y)}{\partial x^2} \text{ and } \frac{\partial q}{\partial y} = \frac{\partial^2 g(x,y)}{\partial y^2} \quad (8)$$

We now define the features based on the *surface gradient derivatives* as two-bit binary representations using zero as the decision boundaries:

$$SGD_x = \tau\left(\frac{\partial p}{\partial x}\right) \text{ and } SGD_y = \tau\left(\frac{\partial q}{\partial y}\right) \quad (9)$$

$$\text{where } \tau(\alpha) = \begin{cases} 1, & \alpha < 0 \\ 0, & \alpha \geq 0 \end{cases} \quad (10)$$

Figure 8 illustrates some sample images representing SGD_x and SGD_y . Although the derivatives of p with respect to the direction y and the derivatives of q with respect to the direction x can also be defined in a similar manner, they may not be as useful as $\partial p/\partial x$ and $\partial q/\partial y$ which correspond to the physical meanings as illustrated in Figure 7. Another related technique, the second partial derivative evaluation utilizes all the four information (i.e. $\partial p/\partial x, \partial p/\partial y, \partial q/\partial x, \partial q/\partial y$) for describing the local curvature of 3D knuckle surface. However, such technique only describes a pixel in one of the four categories: local minimum, local maximum, saddle point, or inconclusive (i.e. can be any of the above three). Besides, our SGD_x and SGD_y feature representation is expected to be more useful than the other two derivatives because of the aforementioned physical interpretation. The *surface gradient derivatives* features not only describe the concavity of irregular knuckle curves and creases but also their orientations (more explanation in section 3.5).

3.5 Feature Matching with Partial Similarity

In order to ensure full potential from the *surface gradient derivatives* features for more accurate matching, a sophisticated matching strategy needs to be formulated for matching binary feature templates. One intuitive approach is to consider the two binary feature templates independently and use the *Hamming Distance* to ascertain their similarity score (represented here as SGD_x only, SGD_y only). The final match score between two 3D finger knuckle images can be computed from the weighted score level combination of such similarity scores. Another efficient approach is to consolidate two binary feature templates into one using *AND* or *OR* operator, and use *Hamming Distance* as the match score between two 3D finger knuckle images (represented here as *1-bit AND*, *1-bit OR*). Besides, the two feature templates can be correspondingly matched with respective probe templates using the *XOR* operator and the resulting *two* pixel-wise similarity templates can be used to generate the similarity score using the *ADD*, *OR* or *AND* operator (represented here as *2-bit ADD*, *2-bit OR*, *2-bit AND*). We performed experiments using the subset of database with the first 30 subjects (each with six forefinger knuckle images in two sessions, results in 180 (30×6) genuine match scores and 5220 ($30 \times 6 \times 29$) imposter match scores) to ascertain comparative performance from several such matching schemes (Figure 9). Please refer to Section 5.1 for more details on the database and experimental protocol. These experiments indicate that our matching scheme (denoted as *Ours final*) and (*1-bit OR*) can achieve two best performing results. The experiments are further extended using 105 subjects (each with 6 images in two sessions, results in 630 (105×6) genuine match scores and 65520 ($105 \times 6 \times 104$) imposter match scores), which validates the effectiveness

of our matching scheme over those from the variations of *Hamming Distance*. It is prudent to analyse the proposed matching strategy in detail and examine the reasons for superior performance.

In order to design an effective feature matching scheme, the nature of features represented in two binary feature templates should be carefully considered. Figure 10 details the nature of features expected to be represented/recovered from the 2-bit feature descriptors at every pixel location. In this figure, value 1 indicates the detection of a line feature (piece-wise linear approximation of knuckle curves or creases) in either vertical or horizontal direction. If no such line features are detected in any of the two direction, it corresponds to a non-line pixel represented by '00'. If a line feature is detected only in SGD_y component, the line feature is expected to have horizontal orientation denoted by '01'. Similarly, a line feature in the vertical orientation is represented by '10'. If such line features are detected in both SGD_x and SGD_y , there can be many possibilities. It could be two intersecting lines in the vertical and horizontal direction. It could also represent a line feature in an arbitrary orientation which is neither nearly vertical or horizontal. This situation is described here as an uncertain line feature and represented '11'.

Conventional approaches for generating similarity scores using binary feature templates use *Hamming Distance* to measure the similarity (represented as outcome 0) or the dissimilarity (represented as outcome 1) when comparing a pair of binary feature values. However, the cases of partial similarity is not accounted in such measurements. Therefore, we introduce an alternative matching scheme to describe the partially matched scenarios. We firstly define perfectly similar outcome (represented as the outcome '0') for three situations when the detected feature represents: (i) a nearly horizontal line '01'; (ii) a nearly vertical line '10'; and (iii) as an uncertain line '11' in *both* the probe and gallery templates. We then define perfectly dissimilar outcomes (represented as the outcome '1') for the two situations when the detected feature (i) does not represent any line '00' in either probe or gallery template, but represents as the line in the other template; and (ii) the detected feature represents a nearly horizontal line '01' in either probe or gallery template but it represents a nearly vertical line '10' in the other template. For the remaining situations, we define partially similar outcome (represented as the outcome 0.5). Let h be this new function which maps two pixelwise *surface gradient derivatives* features into an outcome score, which is represented in Table 2. Let A and B be two surface gradient feature templates of size $M \times N$. Let a_{ij} and b_{ij} ($i \in [1, M], j \in [1, N]$) be the bit-wise surface gradient features in template A and B respectively. The matching score s for computing the distance between the templates A and B is defined as the average of outcome from all feature comparisons:

$$s = \frac{1}{M \times N} \sum_{i=1}^M \sum_{j=1}^N h(a_{ij}, b_{ij}) \quad (11)$$

In order to accommodate pose variations in the acquired

images, best or the minimum of the match scores resulting from the rotational or translational shifting of the probe template can be employed and was also investigated in our experiments.

4. UNIQUENESS OF FINGER KNUCKLE PATTERNS

It is highly desirable to characterize the uniqueness of 3D finger knuckle patterns or estimate the probability that two persons can have substantially similar 3D finger knuckle patterns in a given population. Any such measure to establish uniqueness of 3D finger knuckle patterns can also provide us theoretical upper limit on the expected performance from 3D finger knuckle based biometrics. There are several studies to ascertain theoretical upper limit on the expected performance from other biometric system, *e.g.* using 3D fingerprints [16], iris [33]-[37] or handwriting [38]. Therefore, we attempt to ascertain upper bound on the expected performance from the 3D finger knuckle biometric system presented in this paper.

The uniqueness of 3D finger knuckle patterns can be evaluated from the probability of false matches in a given population, *i.e.*, from the probability of false random correspondence between the finger knuckle representations from the two arbitrary 3D finger knuckle patterns belonging to different fingers. One of the more judicious approach to address this problem is to estimate the number of degrees of freedom [33]-[35]. It is equivalent to computing the maximum number of identities which can be distinguished. Then, the likelihood of two finger knuckle representations from different 3D finger knuckle patterns agreeing completely by *chance* can be computed.

The 2-bit feature descriptor introduced in section 3 consists of four possible representations {'00', '01', '10', '11'} from each of the 3D finger knuckle locations. When two such representations from any pixel locations are compared, there can be three possible outcomes with scores 0, 0.5, or 1. We here make assumption that when two 3D finger knuckle representations from different subjects are matched, the outcome of match scores from the corresponding locations are mutually independent. This independence assumption, similar to as in [16], [27], is justified here as we are interested in theoretical upper bound and as the practical performance is expected to be lower than this estimation after considering such factors involving mutual independence or the noise [29]. Reference [33]-[34] has incorporated binary features for iris biometrics and computed the probability of false random correspondence by modeling the distribution of imposter match scores using a binomial function. Since there are three possible outcomes in our feature representation, a trinomial distribution model consisting of n trials is introduced to model the distribution of imposter match scores. Let p_1, p_2 and p_3 represent the probabilities of having outcome scores 0, 0.5 and 1 respectively. Let X_1 be the random variable representing the number of times outcome 0 is observed over n trials

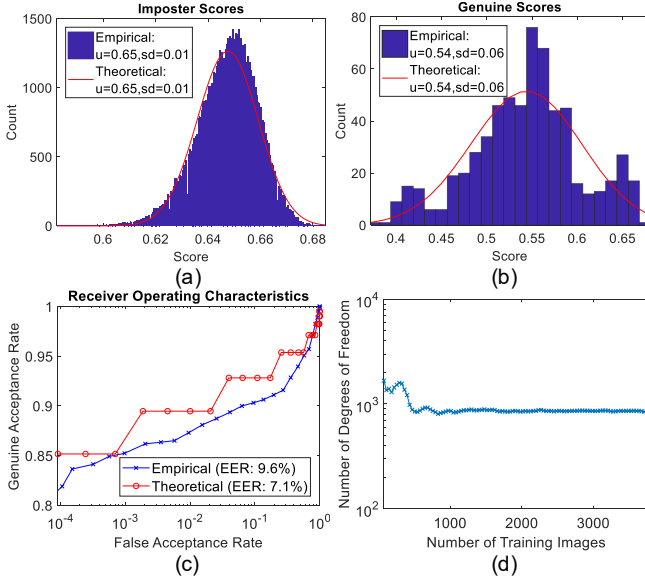


Fig. 11. Empirical and theoretical (a) imposter score distribution, (b) genuine score distribution, (c) the ROC. The influence from the *size* of training set on the estimated number of degrees of freedom is shown in (d).

and x_1 be the value for X_1 from each of such trials. Similarly, we can define X_2, x_2, X_3 and x_3 corresponding to p_2 and p_3 . The probability distribution function corresponding to the trinomial random variables can be expressed as follows:

$$f_{X_1, X_2, X_3}(x_1, x_2, x_3) = \begin{cases} \frac{n!}{x_1! x_2! x_3!} p_1^{x_1} p_2^{x_2} p_3^{x_3} & , \text{ when } x_1 + x_2 + x_3 = n \\ 0 & , \text{ otherwise} \end{cases} \quad (12)$$

and the expectation, variance, and covariance of $X_i, i \in \{1, 2, 3\}$ are:

$$E(X_i) = np_i \quad (13)$$

$$Var(X_i) = np_i(1 - p_i) \quad (14)$$

$$Cov(X_i, X_j) = -np_i p_j \quad (15)$$

Let Y be a random variable representing the match score between two feature representations.

$$Y = 0.5X_2 + X_3 \quad (16)$$

Since the sum of x_1, x_2, x_3 is n , the dependence of x_1, x_2, x_3 can be computed as follows:

$$x_2 = 2(y - x_3) \quad , \quad x_3 \in [0, n] \quad (17)$$

$$x_1 = n - 2y + x_3 \quad , \quad x_3 \in [0, n] \quad (18)$$

Incorporating equations (17)-(18), we can write the probability distribution function for the distribution of scores:

$$f_Y(y) = \begin{cases} \sum_{x_3=0}^n f_{X_1, X_2, X_3}(x_1, x_2, x_3) & , \text{ when } x_1, x_2 > 0 \\ 0 & , \text{ otherwise} \end{cases} \quad (19)$$

with respective expectation and the variance as follows:

$$E(Y) = 0.5E(X_2) + E(X_3) = n(0.5p_2 + p_3) \quad (20)$$

$$Var(Y) = 0.5^2 Var(X_2) + Var(X_3) + Cov(X_2, X_3) \quad (21)$$

$$= n[0.5^2 p_2(1 - p_2) + p_3(1 - p_3) - p_2 p_3] \quad (22)$$

The cumulative distribution function corresponding to (19) represents the false acceptance rate.

Reference [36] details interesting efforts to model transformations from 'true' iris representation to the sensed iris representation using a single bit flip probability. However, such an approach ignores the influence from frequently observed noise introduced from pose and illumination changes during the image acquisition, sensor noise, segmentation errors and some other unknown factors. This is also the plausible reason that the theoretical ROCs presented in [36] do not closely fit with the respective empirical results. Therefore, we did not pursue/incorporate such an approach to formulate our individuality model.

More attractive/realistic approach to model the match score distributions from the binary feature templates appears in [33]-[35]. This approach uses probability distribution function, of the minimum of independent random variables, to model the final match score and is computed from the minimum of scores generated from the rotationally shifted versions of *Iris Code* templates. However, it should be noted that such match scores from the shifted versions are not expected to be completely independent. For instance, the match score between templates A and B is expected to be similar to the match score between template A and the shifted versions of template B when the shift parameter is small (e.g. translated to the left for one pixel). Therefore, such approach will be less accurate when the number of employed shifted versions of the template is large. It should be noted that there are only seven shifted versions of the templates employed in [33]-[35] while there are 39627 shifted versions (from translation and rotations) of the templates in our work. We incorporate a simplified approach to address this problem. The major influence from such operations is to compute minimum match score which results in the shifting of the score distribution. Therefore, we introduce a numerical compensation parameter to accommodate such shifts or to adjust the mean and is estimated during the training stage using the portions of the empirical data. During the training stage, the difference between the mean of the empirical distribution and the theoretical distribution, which is obtained from equation (19), is computed and is defined as the compensation parameter. During the test stage/phase, the final theoretical distribution is obtained from equation (19) using this compensation parameter to accommodate the influence from shifting operations.

In order to theoretically model the distribution of match scores, the number of trails for the trinomial distribution can be computed using the variance obtained from the empirical results. Let σ^2 be such estimated empirical variance. The number of trails n can be computed as follows:

$$\sigma^2 = \frac{Var(Y)}{n^2} \quad (23)$$

$$n = \left\lceil \frac{0.5^2 p_2 (1-p_2) + p_3 (1-p_3) - p_2 p_3}{\sigma^2} \right\rceil \quad (24)$$

Similar to the empirical experiments in Section 5, we generate 65520 ($105 \times 104 \times 6$) imposter match scores from matching the second session images to the first session images, using the feature extraction and matching method described in Section 3.4-3.5, from 105 different subjects, each with 6 images per session. Please refer to Section 5.1 for more details on the database and experimental protocol. The occurrence of four possible representations ('00', '01', '10', '11'), on per pixel basis, can be obtained from this experimental data and used to compute p_1 as 0.1173, p_2 as 0.3116 and p_3 as 0.5711. Therefore, using equation (24), n can be estimated as 886. Similarly, 630 (105×6) genuine match scores can also be used to model the parameters of the same trinomial function for the distribution of genuine match scores. The major difference between the theoretically modeled genuine and imposter score distributions results from the estimated parameters, *i.e.*, p_1, p_2, p_3 and n . In this manner, we can also compute theoretical ROC for the comparison. Figure 11 (a)-(c) presents the comparative illustration of our theoretical and empirical results.

In order to ascertain the reliability of the obtained results, we performed additional experiments by separating the modelling processes into training and test stages. We used first T_n subjects as the training set for computing the probabilities p_1, p_2, p_3 and the number n . The rest of the subjects ($105 - T_n$) are then used as the test set for evaluating the fitting performance. These results are provided in the Appendix A. The close fitting of these empirical results suggest that our trinomial model can quite accurately predict the empirical imposter distribution (the probability of false random correspondence), genuine distribution and ROCs. It can be noted that when T_n becomes larger, less number of samples will be used for the test sets. In this situation, the empirical results are expected to much better, which can result in larger differences between the corresponding theoretical results. It can also be observed from the results in Figure 11 (d) that the number of trials, also referred to as the degrees of freedom, n is quite stable (about 1000) when it is computed using the different size of training sets/data.

In summary, the probability of false random correspondence, the imposter distribution and the false accept rate can be modelled by the trinomial distribution function. The genuine distribution and the false reject rate can also be modelled using similar approach. Our experiments using all the first session images for training have computed n as 886. This suggests that the empirical imposter distribution can be modeled using a trinomial distribution function with 886 trials. Similar to as in [33]-[35], it is reasonable to conclude that each of the finger knuckle feature representation can be modeled with such 886 independent pixels (each with 2 bits). The probability of false random correspondence between finger knuckle representations from any two arbitrary finger knuckle patterns belonging to different fingers is therefore about 4^{-886} or 10^{-533} .

Therefore the probability of false random correspondence is very small, which indicates high uniqueness in the finger knuckle patterns. This probability is much smaller than estimated for the fingerprints [16], [39]. Such difference can be explained from the usage of limited information from (only) the singularity locations or in the extracted minutia feature space, while our feature representation utilizes the information from the entire image.

Table 3. Comparative computational time (in milliseconds).

	Surface Normal Estimation	Depth Integration	Feature Extraction	Total
Surface Code [30]	0.72	0.57	2.77	4.1
Binary Shape [31]	0.72	0.57	0.86	2.2
Ours	0.72	-	0.58	1.3

5 EXPERIMENTS AND RESULTS

5.1 Contactless 3D Finger Knuckle Database

Lack of any 3D finger knuckle images database in the literature has required us to acquire a new dataset using the setup described in section 3.1. Our 3D finger knuckle database has been acquired from more than 130 different subjects and among these 105 subjects have volunteered to provide second session's data. Each of these subjects provided six forefinger 3D knuckle images and six middle finger 3D knuckle images. In our preliminary experiments, it was observed that the forefinger images achieve better performance than using middle finger images. Therefore, forefinger images were employed for the extensive experimental results detailed in this paper. Entire 3D finger knuckle database acquired in this work is made publicly available [40] for further work in this area.

We performed extensive experiments using our proposed method to ascertain effectiveness for the verification and identification problems. These experimental results are presented using the receiver operating characteristics (ROC) curve with equal error rates (EER), and cumulative match characteristics (CMC) curve. We use standard protocol [2], [6], [15], [20] for the two sessions' database. The first session data is used as for the registration or the training while the second session data is used as test set for the performance evaluation. Therefore 630 (105×6) genuine match scores and 65520 ($105 \times 6 \times 104$) imposter match scores were generated. None of the earlier work on the finger knuckle recognition, in the best of our knowledge, has attempted to evaluate the performance for the open set identification problem. However, the deployed biometric systems often have to cope up with unregistered (imposter) user attempts who may be identified as the enrolled users. Such open set identification is widely considered as the more challenging problem and therefore we also performed such evaluation in this work. The first 105 subjects who provided registration data during the first session were considered as enrolled users while the rest of the 25 subjects which only provided one session data were

considered as the unenrolled users. We evaluated the performance with False Negative Identification Rate (FNIR) and False Positive Identification Rate (FPIR). We correct the equations from [42] as in the followings and were used for open set performance evaluation:

$$FPIR(T) = \frac{1}{K} \sum_{i=1}^K H(T - s_{i1}) \quad (25)$$

$$FNIR(T) = 1 - \frac{1}{M} \sum_{i=1}^M H(T - s_{ic}) \quad (26)$$

where T is the threshold; K is the number of searches for non-enrolled images; M is the number of searches for enrolled images; s_{i1} is the score from first rank in i^{th} search; s_{ic} is the score of the true class from i^{th} search; H is the unit step function; and N is the number of enrolled subjects. The equal error rate (EER) corresponding to these two identification rates are also presented.

5.1.1 Comparative Performance Evaluation

Since any effective method for 3D finger knuckle feature description is yet to be developed, we selected the state-of-the-art 3D feature description method, which was originally designed for extracting 3D palm features, as the baselines for comparisons. Two selected methods (*Surface Code* [30] and *Binary Shape* [31]) have shown to be quite effective/accurate for extracting valley and ridge patterns from related hand biometrics. Since both baseline methods require depth images for feature extraction, depth images are computed using *Frankot Chellappa* approach [21] for achieving the best possible performance. Figure 12 shows the comparative experimental results using our *surface gradient derivatives* method (EER=9.6%), *Surface Code* (EER=10.2%) and *Binary Shape* (EER=10.5%). It can be observed from these results that our approach can significantly outperform both of these baselines. These observations validate the arguments and the effectiveness of the *surface gradient derivatives* method detailed in section 3.4 and 3.5 of this paper.

We also comparatively evaluated the computational complexity for our proposed approach with the *Surface Code* [30] and *Binary Shape* [31] approach. In order to fairly ascertain the computational complexity with these competing methods, we ensure that the computational time required for the depth integration and feature extraction is separately illustrated for systematic inspection. In order to ensure consistency and fairness in these comparisons, same pixel resolution of (70×100) was used for both the surface normal vector images and the depth images. The experiments were performed on a machine with Intel Core i7-6700HQ (2.60GHz) using MATLAB 2017b, Windows 10. Table 3 presents the computational time per sample for each of the considered methods. *Frankot Chellappa* approach [21] was employed for the reconstruction using the depth integration. Respective depth images form the input for the feature extraction step as detailed in [30, 31], while surface normal vector images form the inputs for our method. It can be observed that extracting features using *Surface Code* requires the longest computational time since

this method requires demanding computation of curvature and shape index values. Extracting features using our method is the fastest because only simple gradient computations are required. Since our approach bypasses the complex process for the depth integration, the total time required for our approach has further outperformed the baseline methods. It is therefore reasonable to expect that the matching time using the *Binary Shape* features will be smaller than those from our method since there is only one (bit) binary template. Significantly higher matching performance in Figure 12, both for the open and close-set performance evaluation, can justify the effectiveness of our approach over the *Binary Shape* feature method.

Multiple 2D finger knuckle images acquired under single illumination are employed for recovering the 3D finger knuckle images. These 2D images, although noisy with partial illumination, can also be themselves be employed to *simultaneously* improve the performance. The method detailed in reference [20] has shown to offer superior performance over several state-of-the-art feature descriptors introduced in the literature for matching 2D hand images. Therefore, it is a promising baseline method for evaluating the best possible performance from such simultaneously made available 2D finger knuckle images. In this work we employed the publicly available implementation of method in [20] and optimized the parameters for achieving best performance from our segmented finger knuckle images.

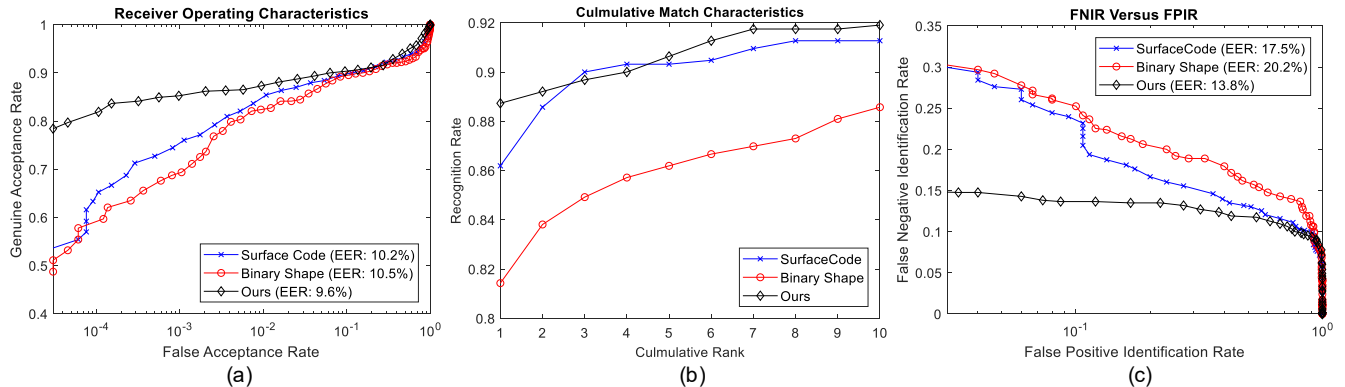


Fig. 12. Comparative experimental results using 3D features on 3D Finger Knuckle Database: (a) ROC; (b) CMC; (c) FNIR versus FPIR.

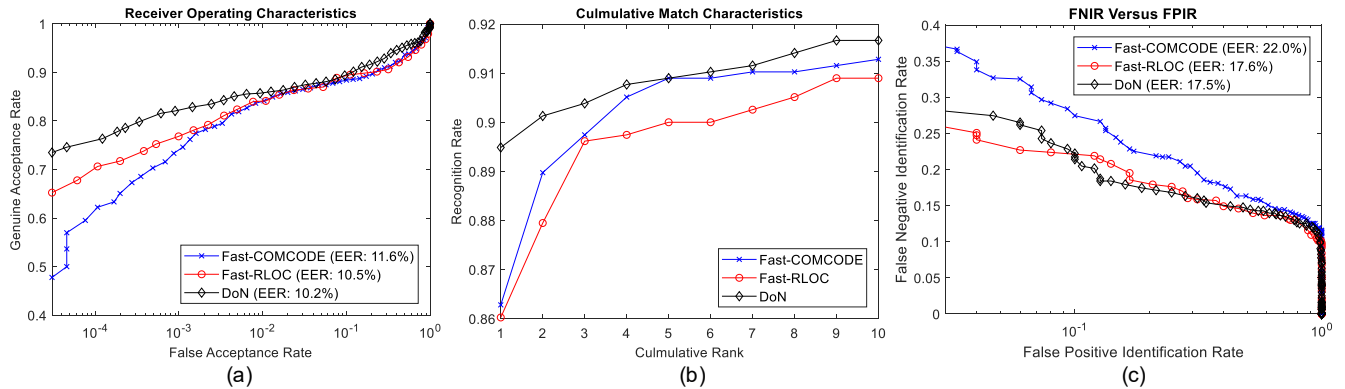


Fig. 13. Comparative experimental results using 2D features on 3D Finger Knuckle Database: (a) ROC; (b) CMC; (c) FNIR versus FPIR.

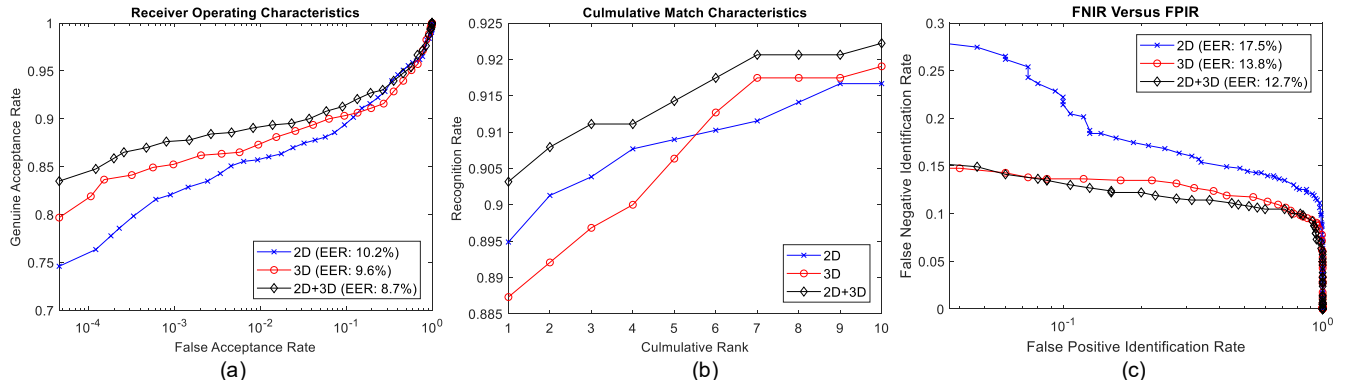


Fig. 14. Comparative experimental results using both 2D and 3D features on 3D Finger Knuckle Database: (a) ROC; (b) CMC; (c) FNIR versus FPIR.

Simultaneous use of such noisy 2D finger knuckle images resulted in 630 (105×6) genuine scores and 65520 ($105 \times 6 \times 104$) imposter scores. The comparative performances using these competing methods can be observed from the ROCs presented in Figure 13. The *DoN* [20] (EER=10.2%) feature descriptor outperforms *Fast-RLOC* [31] (EER=10.5%) and *Fast-CompCode* [31] (EER=11.6%) for matching 2D finger knuckle images.

Combination of simultaneously acquired 3D finger knuckle images and 2D knuckle images can be used to further improve the matching accuracy, which may not be possible by either of these two modalities alone. Therefore, we also performed such experiments to combine match scores, from 3D and 2D finger knuckle images, using the

score level combination. Figure 14 illustrates the results from such combination (EER=8.7%), using our proposed method of 3D finger knuckle matching (EER=9.6%) and the best 2D performing finger knuckle matching using *DoN* (EER=10.2%). Figure 15 illustrates the distribution of 3D and 2D finger knuckle matching scores. It can be observed that in either dimension, it is difficult to separate the genuine scores from the imposter scores. In addition, separating the scores in two classes of 2D matching scores is more difficult than separating those from the 3D matching scores. However, while combining the scores from both dimensions, the task of separating the genuine scores from the imposter scores becomes relatively easier.

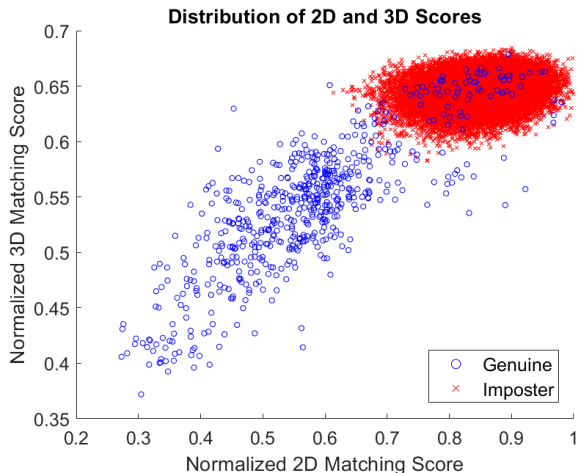


Fig. 15. Distribution of normalized 2D and 3D matching scores.

5.1.2 Detecting Spoof Attacks

The usage of 3D finger knuckle based identification introduced in this paper can offer additional advantage of safeguarding integrity of finger knuckle biometric systems from fraudulent or printed spoof knuckle samples. We performed experiments to ascertain the vulnerability of 2D finger knuckle based biometric systems by simulating print attacks from real subjects as detailed in the following. Firstly, a set of gallery images are acquired. Then, intermediate images are acquired in another session (at least two months) from the respective subjects. These intermediate images are printed as photographs. These printed photographs of finger knuckle images are used for the presentation attacks. During these attacks, it is ensured that the photographs are presented with best possible distance, from the image sensor, to generate images with similar or same scale. Figure 16 illustrates sample 2D and 3D images

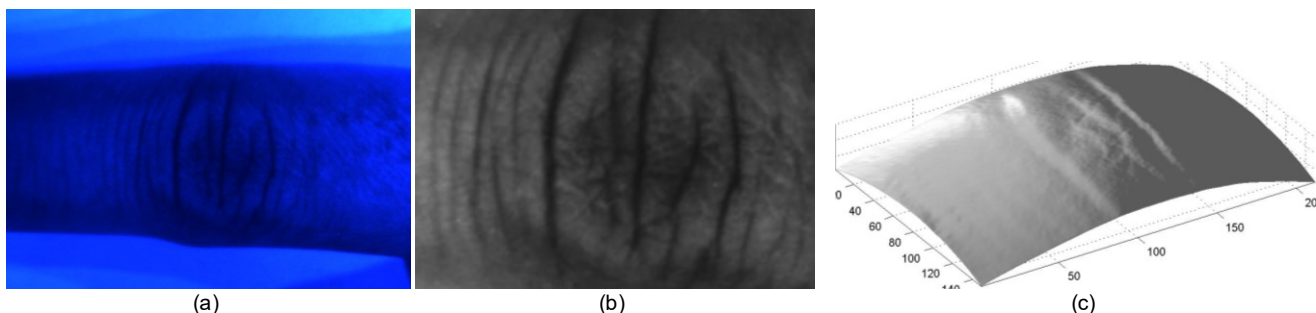


Fig. 16. Sample images from presented photograph to the system: (a) acquired image; (b) resulting 2D image and (c) resulting 3D depth image for the matching.

generated from such presentation attacks using a printed photograph to the system. The probe images were compared with their respective gallery images. The 2D matching scores are computed using the best performing or the *DoN* [20] approach. The 3D matching scores are computed using the proposed *surface gradient derivatives* approach. The decision thresholds corresponding to the respective

Table 4. Dissimilarity scores from the spoof experiments.

Subject ID	2D Matching Score [0,3] (Threshold = 1.1845)		3D Matching Score [0,1] (Threshold = 0.5381)		2D+3D Fusion Score [0,1] (Threshold = 0.5884)	
	Score	Result	Score	Result	Score	Result
1	0.9146	accept	0.6729	reject	0.6603	reject
2	0.9771	accept	0.7082	reject	0.6969	reject
3	0.7199	accept	0.7285	reject	0.6788	reject
4	0.9966	accept	0.7047	reject	0.6967	reject
5	1.2088	reject	0.7194	reject	0.7367	reject
6	1.1189	accept	0.6750	reject	0.6892	reject
7	1.0451	accept	0.6968	reject	0.6968	reject
8	0.9618	accept	0.7129	reject	0.6986	reject
9	1.0160	accept	0.7050	reject	0.6995	reject
10	0.7707	accept	0.6771	reject	0.6444	reject

EERs were automatically chosen for the experiments. These experimental results are summarized in Table 4. When only 2D information are used, 9 out of 10 samples can bypass the system, which implies that the fake identities corresponding to the presentation attacks cannot be detected. It can also be observed from this table that when only 3D information is used, none of the presented samples can bypass the system, enabling the detection of fake identities to protect integrity of the system. When both the 2D and 3D information is incorporated, the results are the same as those from only using the 3D information. Unlike fraudulent/covert acquisition of 2D finger knuckle photographs, acquisition of 3D finger knuckle patterns is extremely difficult as it requires the user to intentionally present his/her finger under a complex 3D imaging system. In summary, our experiments indicate that 3D finger knuckle based biometric system offers significantly enhanced security to protect the integrity of system from the fake or fraudulent finger knuckle samples.

5.2 Other Experimental Results

This section details the additional experiments using *publicly* available 3D palmprint and 3D fingerprint databases to further ascertain effectiveness of our 3D feature matching approach detailed in section 3.4-3.5. The 3D palmprint

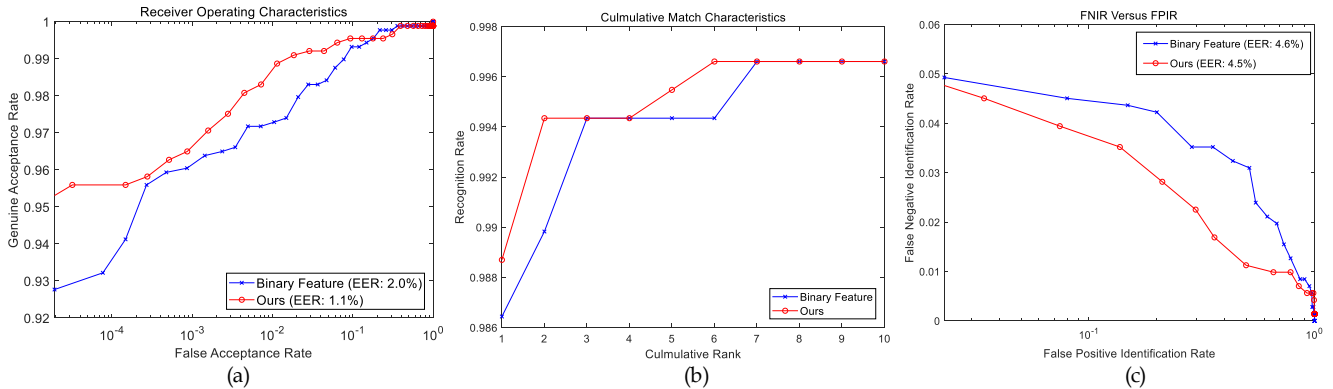


Fig. 17. Comparative experimental results using 3D features using contactless 3D palmprint database: (a) ROC; (b) CMC; (c) FNIR versus FPIR.

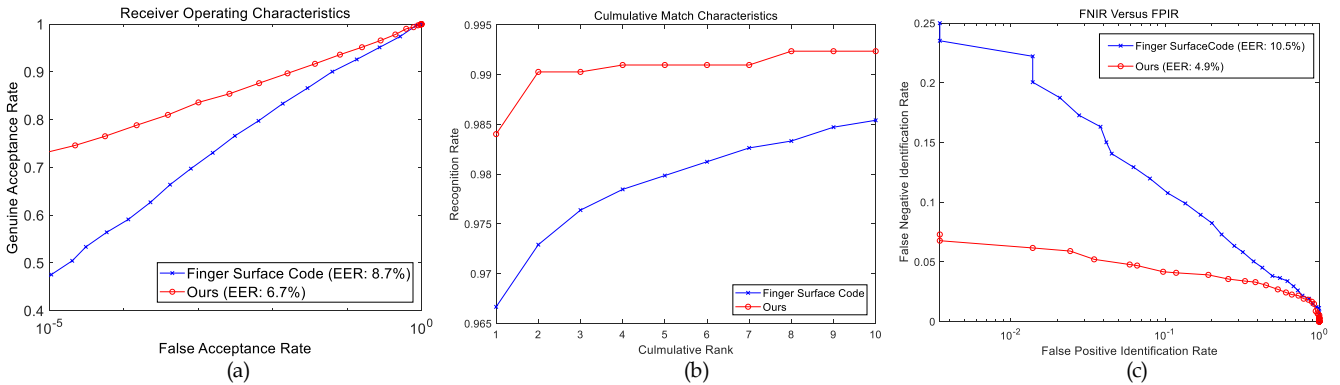


Fig. 18. Comparative experimental results for matching 3D finger surfaces using 3D Fingerprint Database: (a) ROC; (b) CMC; (c) FNIR versus FPIR.

database provided from [30] contains 1770 palmprint images from 177 different subjects in two sessions. There are five 3D images for each subject per session. We have evaluated our proposed method using all images. First session images are used as training sets while second session images are used as testing sets, which results in 885 (177×5) genuine and 155760 ($177 \times 176 \times 5$) imposter matching scores. To account for the translation variations in this database, the templates are shifted with vertical and horizontal translations. The minimum score is considered as the final score. For the open set evaluation on the performance of identification rates, 142 subjects (80%) are considered as enrolled users while the remaining 35 subjects (20%) are considered as unenrolled users. Since neither surface normal images or photometric stereo 2D images are available, we compute the surface normal images from the 3D images by using a simple gradient method. Our method is compared with the state-of-the-art method (*Binary Shape*) [31] on this database, which is also reported superior performance than *Surface Code* [30]. It can be observed that the *Binary Shape* method incorporates a masking procedure which is not provided in their implementation. However, the details are not clearly presented. In order to ensure fairness in comparison, the evaluation on both *Binary Shape* and our method are without masks. Comparative results in Figure 17 indicates that our surface gradient derivatives features (EER of 1.1%) can also offer outperforming results over the *Binary Shape* (EER of 2.0%) approach for the 3D palmprint matching.

Furthermore, a template size of (128×128) with 1-bit is required for *Binary Shape* method, while only a template size of (64×64) with 2-bits is required for our method for obtaining the optimal performance. Therefore, our method also outperformed *Binary Shape* with much higher efficiency via the reduction of template sizes.

The *surface gradient derivatives* approach introduced in this work is quite effective for frequent concave and convex-like 3D patterns which generally exists in finger knuckle. However, the density of such concave and convex patterns is sparse and less pronounced in 3D palmprint images. Besides, the central region of 3D palm surface is largely concave. This can degrade the accuracy from our feature descriptor in encoding the palm line features. Therefore, our feature descriptor is expected to be less effective for encoding features from 3D palm surface than those from 3D finger knuckle patterns. In the 3D palm database, the surface normal information was computed from the noisy depth images which is another plausible reason for some degradation in performance using the surface gradient derivatives features. Despite the above challenges, our proposed approach has still shown outperforming results for the contactless 3D palm database.

Another public database from contactless 3D fingerprint is available from [16], [27] and was also attempted to ascertain comparative performance for matching 3D fingerprint surfaces. This database provides 1560 3D fingerprints, reconstructed using 10920 2D fingerprint images,

obtained from 260 clients. In order to fairly compare with the performance reported in [16], [27] for matching finger surface, the same evaluation protocol was adopted. Such matching of 3D finger surfaces from 240 clients, each with six images, resulted in 3600 ($240 \times C_2^6$) genuine and 1032480 ($C_2^{240} \times 6 \times 6$) imposter matching scores. In order to account for the translation variations in this database, the templates were shifted with vertical and horizontal translations. The minimum score obtained from such shifting was considered as the final match score. For the open set evaluation on the performance of identification rates, 192 clients (80%) were considered as the enrolled users while remaining 48 subjects (20%) were considered as unenrolled users. Figure 18 illustrates the comparative experimental results, using the state-of-the-arts pixelwise feature descriptor (*Finger Surface Code* [27] with *Frankot Chellappa* approach [21]), which was also reported to be superior or outperforming in [27] than the *Surface Code* [30]. It can be observed from these results that the proposed *surface gradient derivatives* feature approach significantly outperforms the baseline results.

It is well known that state-of-the-art feature descriptors for fingerprint images incorporate minutiae features. In this paper, our experiments demonstrated that the usage of proposed *surface gradient derivatives* features can achieve outperforming results over the state-of-the-art pixelwise feature descriptors. The usage of surface singularities or non-pixelwise feature descriptors for matching 3D finger knuckle patterns is highly desirable in further extension of this work.

6 SUMMARY AND FURTHER WORK

Currently available online finger knuckle identification systems only incorporate discriminative 2D information for the user identification. This paper has investigated the development of a 3D finger knuckle identification system and also introduced 3D finger knuckle images database, for the first time in the literature, for the further research. Any direct application of existing 3D feature descriptors, like those developed for the 3D palmprint or 3D fingerprint identification, is not expected to recover most discriminative features from the 3D finger knuckle patterns. Therefore, the development of specialized feature descriptors is critical to realize full potential from 3D finger knuckle biometrics. The feature descriptor introduced in section 3.4 of this paper addresses such objective and has shown to offer outperforming results. One of the fundamental questions relating to any new biometric modality relates to its uniqueness, or individuality of the finger knuckle biometrics, which has not yet been studied in the literature. This paper has attempted to address this problem by developing the individuality model for 3D finger knuckle patterns using the best performing feature descriptor.

Despite the advantages from the 3D finger knuckle

identification, the deployment of a 3D finger knuckle identification system is more complex than that of a 2D finger knuckle identification system. Such increase in complexity, over 2D systems, is largely due to the reconstruction or acquisition of 3D finger knuckle images. Among the existing 3D imaging technologies such as laser scanning, multi-view stereo, and structured lighting, our proposed new system adopted the photometric stereo approach due to its low cost, high quality imaging and simple deployment. This approach only requires a single fixed camera with at least three light sources, while more light sources may enhance the reconstruction accuracy. The key limitation of such approach lies in its sensitivity towards the ambient illumination. Therefore, efforts are required to appropriately position the camera, select and fix the illuminators, which reduce the adverse influence from ambient illumination during the imaging. Such shortcomings are however worthy for the tradeoff of more accurate recognition and anti-spoofing performance, as also indicated from our results in the paper.

Our work/attempt to systematically evaluate the potential from 3D finger knuckle patterns for the biometric identification has achieved promising results. A lot more work however needs to be done to realize full potential from this biometric identifier. Recovery of non-pixel-wise features or those based on the singularity of patterns, such as the minutiae features employed for matching fingerprints, is expected to be more effective (for higher accuracy and efficiency) than pixel-wise features and should be pursued in further extension of this work. Our attempts to achieve further performance improvement by incorporating popular deep learning based methods were not effective and their performance is limited by the size of training data which is the key challenge for 3D finger knuckle data employed in this work. The individuality model presented in this paper has made assumptions on the mutual independence of match scores and has been justified as such model can provide theoretical upper limit on the performance expected from the 3D finger knuckle patterns. Incorporating interdependence of features, or the scores during feature extraction process, can provide more realistic estimates on the individuality and is suggested in the further extension of this work.

REFERENCES

- [1] M. Tistarelli, Stan Z. Li, R. Chellappa (Eds.), "*Handbook of Remote Biometrics: for Surveillance and Security*", 2nd Edition, Springer Verlag London, 2019.
- [2] D. Maltoni, D. Maio, A. Jain, and S. Prabhakar, "*Handbook of Fingerprint Recognition*", Springer-Verlag London, 2009.
- [3] "Summary of NIST standards for biometric accuracy, temper resistance and interoperability", *NIST Report*, 2002. https://www.nist.gov/sites/default/files/documents/2016/12/21/nistapp_nov02.pdf
- [4] "Role of biometric technology in Aadhaar authentication", *Authentication Accuracy Report*, UIDAI, March 2012.

- http://stateofaadhaar.in/wp-content/uploads/UIDAI_Role_2012.pdf
- [5] K. Sricharan, A. Reddy and A. G. Ramakrishnan, "Knuckle based hand correlation for user verification," *Proc. SPIE* vol. 6202, 2006. doi: 10.1117/12.666438
 - [6] A. Kumar and Ch. Ravikanth, "Personal authentication using finger knuckle surface", *IEEE Trans. Info. Forensics & Security*, vol. 4, no. 1, pp. 98-110, Mar. 2009.
 - [7] G. Jaswal, A. Kaul, and R. Nath, "Knuckle print biometrics and fusion schemes – overview, challenges, and solutions," *ACM Transactions. ACM Computing Surveys*, Vol. 49, No. 2, Article 34, Nov. 2016
 - [8] L. Zhang, L. Zhang, D. Zhang and H. Zhu, "Online finger-knuckle-print verification for personal authentication," *Pattern Recognition*, vol. 43, no. 7, pp. 2560-2571, Jul. 2010.
 - [9] Q. Zheng, A. Kumar, and G. Pan, "Contactless 3D fingerprint identification without 3D reconstruction," *Proc. Intl. Workshop Biometrics & Forensics*, Alghero, Italy, June 2018.
 - [10] L.-q. Zhu, and S.-y. Zhang Multimodal biometric identification system based on finger geometry, knuckle print, and palm print," *Pattern Recognition Letters*, pp. 1641-1649, Sep. 2010.
 - [11] D. L. Woodard and P. J. Flynn, "Finger surface as a biometric identifier", *Computer Vision and Image Understanding*, vol. 100, no. 3, pp. 357-384, Dec. 2005
 - [12] J. J. Koenderink and A. J. Vandoorn, "Surface shape and curvature scales," *Image & Vision Comp.*, no. 8, pp. 557-564, Oct 1992.
 - [13] C. Dorai and A. K. Jain, "COSMOS - A representation scheme for 3D free-form objects," *IEEE Tran. Pattern Anal. Mach. Intell.*, vol. 19, no. 10, pp. 1115-1130, Oct 1997.
 - [14] Y. Wang, Q. Hao, A. Fatehpuria, D. L. Lau, and L. G. Hassebrook, "Data acquisition and quality analysis of 3-dimensional fingerprints" *Proc. IEEE Conf. Biometrics, Identity and Security*, Tampa, Sp. 2009.
 - [15] P. Yan and K. W. Bowyer, "Biometric recognition using 3D ear shape," *IEEE Tran. Pattern Anal. Mach. Intell.*, vol. 29, no. 8, pp. 1297-1308, Aug 2007.
 - [16] A. Kumar and C. Kwong, "Towards contactless, low-cost and accurate 3d fingerprint identification," *IEEE Tran. Pattern Anal. Mach. Intell.*, vol. 37, no. 3, pp. 681-696, 2015.
 - [17] K. I. Chang, K. W. Bowyer, and P. J. Flynn, "An evaluation of multimodal 2D+3D face biometrics," *IEEE Tran. Pattern Anal. Mach. Intell.*, vol. 27, no. 4, pp. 619-624, Apr 2005.
 - [18] K. Ito, T. Aoki, H. Nakajima, K. Kobayashi, T. Higuchi, "A palmprint recognition algorithm using phase-only correlation," *IEICE Trans. Fundamentals of Electronics, Communications and Computer Sciences*, vol. E91-A, pp. 1023-1030, April 2008.
 - [19] A. Shoichiro, K. Ito, and T. Aoki, "A multi-finger knuckle recognition system for door handle," *Proc. 6th IEEE Intl. Conf. Biometrics: Theory, Applications and Systems*, BTAS 2013, Sep. 2013.
 - [20] Q. Zheng, A. Kumar, and G. Pan, "A 3D feature descriptor recovered from a single 2D palmprint image," *IEEE Tran. Pattern Anal. Mach. Intell.*, vol. 38, no. 6, pp. 1272-1279, Jun 2016.
 - [21] R. T. Frankot and R. Chellappa, "A method for enforcing integrability in shape from shading algorithms," *IEEE Tran. Pattern Anal. Mach. Intell.*, vol. 10, no. 4, pp. 439-451, Jul 1988.
 - [22] T. Simchony, R. Chellappa, and M. Shao, "Direct analytical methods for solving Poisson equations in computer vision problems," *IEEE Tran. Pattern Anal. Mach. Intell.*, vol. 12, no. 5, pp. 435-446, May 1990.
 - [23] R. J. Woodham, "Photometric-method for determining surface orientation from multiple images," *Optical Engineering*, vol. 19, no. 1, pp. 139-144, 1980.
 - [24] A. Kumar and Z. Xu, "Personal identification using minor knuckle patterns from palm dorsal surface," *IEEE Trans. Info. Forensics & Security*, vol. 11, pp. 2338-2348, Oct. 2016.
 - [25] R. T. S. Ikehata and K. Aizawa, "Photometric stereo using constrained bivariate regression for general isotropic surfaces," *Proc. CVPR 2014*, pp. 2187-2194, 2014.
 - [26] S. Ikehata, D. Wipf, Y. Matsushita, and K. Aizawa, "Robust photometric stereo using sparse regression," *Proc. CVPR 2012*, pp. 318-325, 2012.
 - [27] A. Kumar and C. Kwong, "Towards contactless, low-cost and accurate 3D fingerprint identification," *Proc. IEEE Intl. Conf. Computer Vision & Pattern Recognition*, Proc. CVPR 2013, pp. pp. 3438-3443, Portland, June 2013
 - [28] B. X. Shi, P. Tan, Y. Matsushita, and K. Ikeuchi, "Bi-polynomial Modeling of Low-Frequency Reflectances," *IEEE Tran. Pattern Anal. Mach. Intell.*, vol. 36, no. 6, pp. 1078-1091, Jun 2014.
 - [29] S. C. Dass, "Assessing fingerprint individuality in presence of noisy minutiae", *IEEE Trans. Info. Forensics & Security*, vol. 5, no. 1, pp. 62-70, 2010.
 - [30] V. Kanhangad, A. Kumar, and D. Zhang, "A Unified Framework for Contactless Hand Verification," *IEEE Trans. Info. Forensics & Security*, vol. 6, no. 3, pp. 1014-1027, Sep 2011.
 - [31] Q. Zheng, A. Kumar, and G. Pan, "Suspecting Less and Doing Better: New Insights on Palmprint Identification for Faster and More Accurate Matching," *IEEE Trans. Info. Forensics & Security*, vol. 11, no. 3, pp. 633-641, Mar 2016.
 - [32] A. Kumar, *Contactless 3D Fingerprint Identification*, Springer Nature Switzerland AG, 2018.
 - [33] J. Daugman, "High confidence visual recognition of persons by a test of statistical independence," *IEEE Tran. Pattern Anal. Mach. Intell.* vol. 15, no. 11, pp. 1148-1161, Nov 1993.
 - [34] J. Daugman, "The importance of being random: statistical principles of iris recognition," *Pattern Recognition*, vol. 36, pp. 279-291, Feb 2003.
 - [35] J. Daugman, "Information theory and the iriscodes," *IEEE Trans. Info. Forensics & Security*, vol. 11, no. 2, pp. 400-409, 2016.
 - [36] R. M. Bolle, S. Pankanti, J. H. Connell, and N. K. Ratha, "Iris individuality: A partial iris model," *Proc. 17th Intl. Conf. Pattern Recognition*, vol 2, pp. 927-930, 2004.
 - [37] B. Li, Z. F. Yan, W. M. Zuo, and F. Yue, "Modeling the Individuality of Iris Pattern and the Effectiveness of Inconsistent Bit Masking Strategy," *Proc. IEEE Intl. Conf. Identity, Security and Behavior Analysis*, 2015.
 - [38] S. N. Srihari, S. H. Cha, H. Arora, and S. Lee, "Individuality of handwriting," *J. Forensic Sciences*, vol. 47, pp. 856-872, Jul 2002.
 - [39] S. Pankanti, S. Prabhakar, and A. K. Jain, "On the individuality of fingerprints," *IEEE Tran. Pattern Anal. Mach. Intell.* vol. 24, no. 8, pp. 1010-1025, Aug 2002.
 - [40] The Hong Kong Polytechnic University Contactless 3D Finger Knuckle Images Database, <http://www.comp.polyu.edu.hk/~csajaykr/3DKnuckle.htm>, 2019.

- [41] A. Kumar, "Importance of being unique from finger dorsal patterns: Exploring minor finger knuckle patterns in verifying human identities," *IEEE Trans. Information Forensics & Security*, vol. 9, pp. 1288-1298, Aug. 2014
- [42] P. Grother and M. Ngan, "The IJB-A Face Identification Challenge Performance Report," *NIST Report*, 2017.

Appendix A

This appendix refers to Section 4 of this paper and provides additional experimental results by separating the modeling processes into training and test stages. We used first T_n subjects data as the training set for computing the probabilities p_1 , p_2 , p_3 and the number of trials n . The rest of the subjects ($105 - T_n$) are then used as the test set for evaluating the performance.

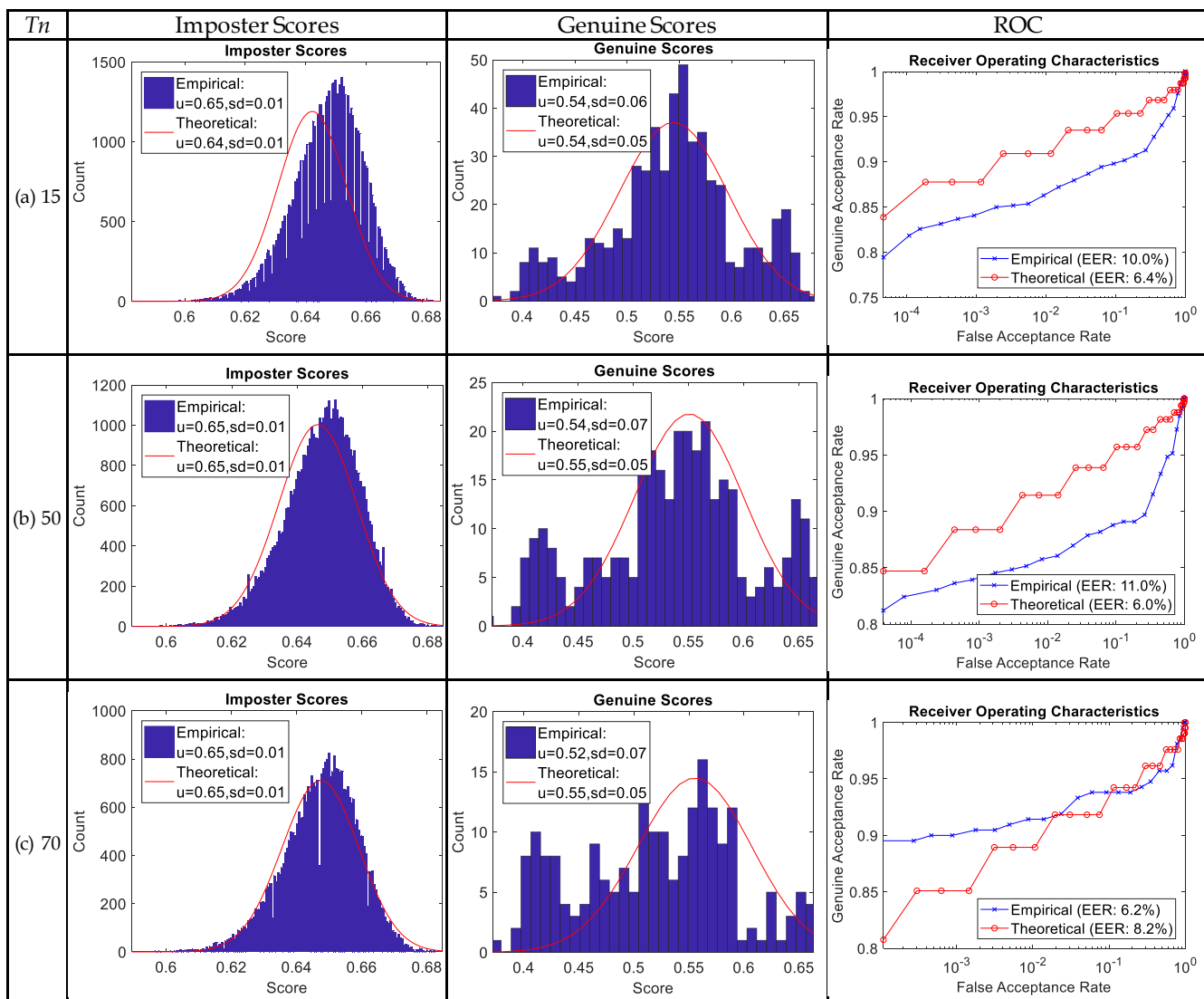


Fig. A1. Empirical and theoretical score distribution from split training and test set with (a) 15, (b) 50, (c) and 70 subjects used for the respective training.